*J. Fluid Mech.* (1993), *vol.* 246, *pp.* 675–691



# Vorticity measurements in the near wake of a circular cylinder at low Reynolds numbers

By R. B. GREEN† AND J. H. GERRARD
Department of Engineering, University of Manchester, Oxford Road, Manchester M13 9PL, UK

(Received 25 July 1991 and in revised form 24 August 1992)

The technique of the particle streak method has been applied to the study of bluff-body wakes at low Reynolds number. Vorticity and shear stress were measured to an accuracy of 15–20%. The vortex shedding cycles at Reynolds number of 73 and 226 are shown and the differences between the two are highlighted. Quantitative descriptions of the previously described vortex splitting phenomenon in the near wake are made, which leads to a description of the vortex shedding mechanism at low Reynolds number. The definition of low-Reynolds-number formation region length is examined. The strength of shed vortices obtained from integration of the vorticity is compared with directly measured vortex strengths and with the results of two-dimensional numerical analysis.

## 1. Introduction

The role of the near wake in the bluff-body vortex shedding mechanism is an important one and has been the subject of considerable scrutiny. The ultimate aim in studying the vortex formation region is to understand how a shed vortex forms. With the aid of flow visualization and numerical analysis, Gerrard (1966, 1967) was able to describe the vortex shedding mechanism above Reynolds numbers ($Re$) of around 500 in the following terms: The forming vortex remains stationary relative to the cylinder as it grows. At the same time it draws the shear layer from the other side of the wake across the wake centreline, eventually cutting off the supply of vorticity to the growing vortex and thus determining the shedding frequency. Figure 1 shows a schematic diagram of the vorticity entrained by the growing vortex from the other side of the wake. Vorticity 'a' is entrained into the growing vortex, vorticity 'b' is entrained into the separated shear layer, and vorticity 'c' moves back towards the cylinder where it is cancelled in the next half of the shedding cycle. Thus, the path of vorticity 'b' is of key importance in Gerrard's hypothesis.

The present problem is concerned with the behaviour of the near wake at lower Reynolds numbers. At the lowest $Re$ considered there is only a very small crossflow in the near-wake region, and the vortex shedding mechanism is characterized by a 'vortex splitting action' (Freymuth, Finaish & Bank 1986). Vortices appear to split apart as they are shed and there is an extensive region of flow back towards the cylinder. This process has also been observed by Gerrard (1978). Substantial crossflow does not exist until some distance downstream (the lower the $Re$, the greater the distance), and therefore Gerrard's hypothesis does not apply at low $Re$.

No adequate definition of the formation region length at low $Re$ exists, which is a

† Present address: Department of Aerospace Engineering, University of Glasgow, UK.

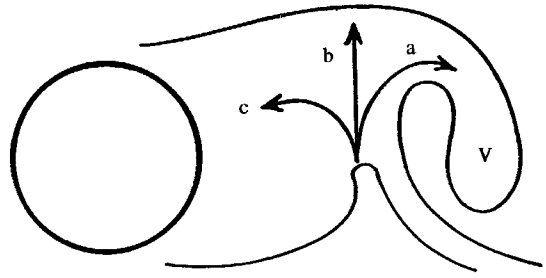


FIGURE 1. Sketch of the entrainment process in the near wake at high Reynolds number. The vortex, V, remains stationary relative to the cylinder whilst growing, a, b and c denote transport of vorticity.

consequence of the incomplete understanding of the near-wake region. The formation region is the area of the near wake where vortex shedding is initiated, and the formation length is a measure of its size in the streamwise direction. Bloor (1964) defined it in terms of the cross-flow at high $Re$. At low $Re$, Gerrard (1978) defined it in terms of the approach of the flow to the rear surface of the cylinder, thus accounting for the features associated with low-$Re$ vortex shedding. At these $Re$, rates of diffusion and convection of vorticity in the near wake are comparable, so a definition based purely on flow visualization (like Gerrard's 1978) is not strictly speaking sufficient and a definition based on vorticity is more appropriate. It has been suggested that the formation length can be defined in terms of the maximum r.m.s. longitudinal velocity fluctuation at the vortex shedding frequency. At low Reynolds numbers the part of the vortex which is eventually shed becomes more compact as it progresses down the formation region. We will show, however that the maximum velocity fluctuation definition still applies. Crossflow is the salient feature of high-$Re$ vortex shedding. When a cylinder oscillates transversely to the free-stream direction a crossflow relative to the cylinder is induced and at large amplitudes the higher-$Re$ type of vortex formation is observed at low $Re$.

In view of the above descriptions, the need to measure vorticity in the near wake at low $Re$ arises, which is the main subject of the present paper. Vorticity measurements for this type of flow are difficult. Because of the unsteady nature of the flow it is preferable that the velocity (and hence vorticity) be measured over the whole of the flow field instantaneously, and the Particle Stream Method (PSM) is well suited to this type of problem. Imaichi & Ohmi (1983) used PSM to measure the instantaneous vorticity field in the near wake at $Re = 100$. They did not, however, offer a great deal of interpretation of their results. Their approach involved manually locating the particle streaks (i.e. the velocity vectors) on a photographic film, although further processing was done digitally. Since the flow field may contain many velocity vectors, this approach is tedious, which ultimately restricts the range of $Re$ that can be tested. The present paper describes a technique where the manual processing burden is virtually eliminated. This is achieved through extensive use of real-time digital image processing hardware and software. Cylinder models were towed along a specially designed water tank and the motions of small particles floating at the water surface were recorded onto video tape for further analysis. Vorticity contours inside a $4D$ long by $3D$ wide area just behind the rear surface of a circular cylinder of diameter $D$ were measured in the range $73 < Re < 226$. The overall accuracy of the technique was found to be comparable to that of the contemporary PSM techniques. Viscous shear stress was also determined from the

measured velocity field. A vortex shedding mechanism is described in terms of the vorticity field and a definition of formation region length is consequently proposed.

## 2. Experimental technique

The apparatus used in the PSM experiment consisted of three parts: the light source and illumination system, the water tank and model towing system, and the image recording/analysis system. Descriptions of the individual items follow: a more complete description is given by Green (1989).

The light source was a 10 mW Helium-Neon laser which was fixed rigidly onto an optical bench. The laser beam was levelled to horizontal and shone parallel to the bench. The beam was reflected off a vertical axis cylindrical mirror to form a thin sheet of light in the horizontal plane. This whole piece of apparatus was positioned alongside the working section of the water tank, with the plane of the light sheet at the same level as the water surface so that the light shone along it.

The water tank was 4 m long by 75 cm wide by 40 cm deep. It was manufactured from glass reinforced plastic, apart from the ends and the working section which were made of transparent Perspex. The working section was positioned at the centre of the tank and was 43 cm long. To minimize heat transfer to the water in the tank (and therefore reduce background motions) the Perspex sections of the tank were double glazed and the remaining side and bottom surfaces were insulated by a paper-filled cavity. Evaporation was minimized by covering the tank with a well-fitting lid. The whole of the tank was supported by a sturdy steel framework and was situated in a temperature-controlled laboratory.

The model towing system consisted of an electric motor coupled through a 500:1 reduction gear box and electrical clutch to a drive wheel. The motor system was placed at one end of the tank. An inextensible fibre-based tape, looped around the drive wheel and an idling wheel at the other end of the tank, was fastened onto a towing carriage which rolled smoothly on highly polished steel rails. A 12.7 mm diameter circular cylinder model was suspended from the carriage and was held in the water with its lower (flat) end at 2 mm from the bottom of the tank. This small gap size was essential to ensure straight and parallel shedding (Slaouti & Gerrard 1981). The overall model aspect ratio was 28. This particular experimental facility has been described elsewhere by Anagnostopoulos & Gerrard (1976), Gerrard (1978), Slaouti & Gerrard (1981) and Al-Khafaji (1989).

Pliolite, ground and sieved to an average diameter of 150 μm was used to seed the flow. It was mixed with water and sprayed onto the water surface in a fine mist just prior to the start of the run. Using this technique, the particles floated below and in contact with the water surface, where they were illuminated by the laser sheet.

A Pulnix monochrome $256 \times 256$ pixel CCD camera was mounted on the towing carriage and was focused on the relevant area just behind the rear surface of the cylinder model. Live images from the camera were recorded directly onto high-quality video tape. Real-time image processing was done by playing the recorded motions back through an Oculus 400-FG real-time image digitiser. A 12 MHz personal computer acted as a central processor. The image digitizer binarized the incoming images so that illuminated particles appeared as white on a black background. Real-time image processing software then performed logical OR (which has the effect of multiple exposure) over a specifiable time interval so that a moving particle appeared as a thin white streak, whose length was proportional to the local instantaneous velocity. To analyse the pictures, software to identify individual

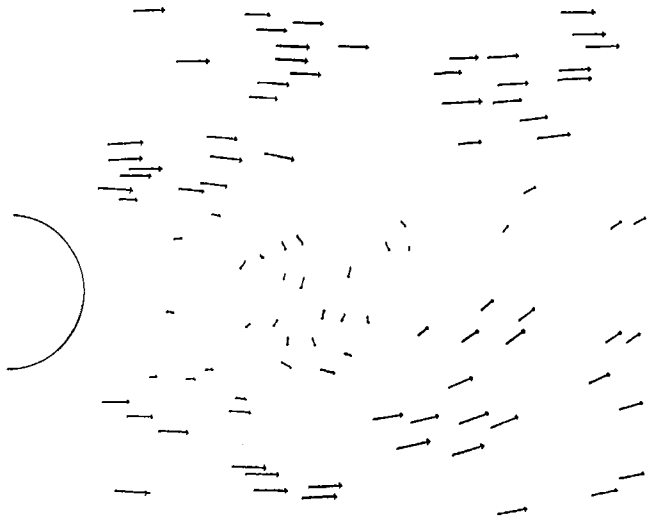

FIGURE 2. Velocity vectors (streak lines) at a Reynolds number of 73. Cylinder diameter is 12.7 mm. Streak grab time is 450 ms.

particle streaks and to calculate their lengths and angles to the direction of the cylinder motion were used. A 180° ambiguity in the direction of each velocity vector remained, which was resolved manually.

## 3. Method and preliminary image analysis

A careful procedure was adopted prior to each run. Firstly, the water surface was cleaned about 3 hours before a run by placing a few drops of detergent on the water surface at one end of the tank and sucking away the debris at the other. The rails and wheels were then polished to ensure that the carriage ran smoothly. About an hour before a run, the motor speed was set at the required value. The laser sheet was then adjusted to the final position (so that it shone parallel to and was just grazing the water surface). Just before the run, the tank lid was removed and the Pliolite/water mixture was sprayed onto the surface. The run was then started and the particle motions were recorded onto video tape as the cylinder model ran through the working section.

After the run, the image analysis procedure was started. The video recording was played back and the shedding frequency was measured. The tape was then played back through the image digitizer which was pre-programmed to sample five frames of particle streaks separated by one tenth of a shedding period. A streak sampling time was typically 0.3 times one tenth of the shedding period. For each frame sampled, an additional frame was sampled one shedding period later. Further analysis was as follows.

(i) Background 'noise' pixels, defined as isolated pixels, were removed from the sampled pictures.

(ii) Individual particle streaks were identified.

(iii) The streaks were approximated to rectangles of equivalent area and second moments of area. Thus the lengths and the angles of the streaks to the free-stream flow were calculated.

(iv) The 180° ambiguity in the velocity vector was settled manually. This was the

only manual part of the analysis procedure, although use of the personal computer considerably eased the burden.

The image analysis procedure together with the computational algorithms are described in further detail by Green (1989).

## 4. Calculation of vorticity

The velocity vectors from an analysis of a single frame at $Re = 73$ are shown in figure 2. The rear surface of the cylinder is shown at the left of the picture and the flow is from left to right. To increase the number of velocity vectors in the picture the velocity vectors from the frame sampled one shedding period later were superimposed onto it. This result is shown in figure 3. The accuracy implications are assessed later in this section.

Vorticity is defined as $\zeta = \partial v/\partial x - \partial u/\partial y$.

For discrete data, the vorticity has to be found numerically. Since the velocity vectors in figure 3 are randomly distributed, they first have to be interpolated onto a regular grid of points.

An interpolation scheme described by Agüí & Jiménez (1987) was chosen for the present application. The velocity $(u_j, v_j)$ at the position $(x_j, y_j)$ of the centre of the vector is given by:

$$u_j = \sum_{k=1}^{n} u_k \exp(-r_k^2/H^2) \Big/ \sum_{k=1}^{n} \exp(-r_k^2/H^2),$$

$$v_j = \sum_{k=1}^{n} v_k \exp(-r_k^2/H^2) \Big/ \sum_{k=1}^{n} \exp(-r_k^2/H^2),$$

where $n$ is a suitable number of velocity vectors, and $r_k$ is the distance of the velocity vector $k$ from the point $j$ onto which it is being interpolated. $H$ is the window width, which determines the relative contribution of each measured velocity vector to the interpolated velocity.

A series of numerical experiments were performed to assess the accuracy of the technique and the factors which determined the value of $H$. The procedure involved numerically 'seeding' an Oseen vortex (whose velocity field is known) to create a field of randomly distributed velocity vectors, which were then interpolated onto a regular grid using the above interpolation scheme. The interpolated vectors were then compared to the known velocity vectors, and the performance assessed in terms of the root mean square of the differences between the interpolated values and the known values. As expected the accuracy was strongly dependent upon $H$, although near to the optimum value, the accuracy varied only slightly with $H$. The optimum value of $H$ was found to be proportional to the number of seeded vectors, as suggested by Agüí & Jiménez (1987). Finally, the optimum accuracy depended upon the number of seeding vectors. For 80 vectors, the r.m.s. deviation was 8%, while for 200 vectors it was 4%. Thus, even for a small number of vectors, the accuracy is respectable, although as large a number as possible is preferable.

To enhance the interpolation scheme, the number of velocity vectors was artificially increased by superimposing the vectors from two sampled frames separated in time by exactly one shedding cycle (as described earlier); increasing the number of vectors by increasing the particle seeding density in the flow was found to be counter-productive, since the particle streaks tended to merge together and direct image analysis was made difficult. All results cited from now on are for the

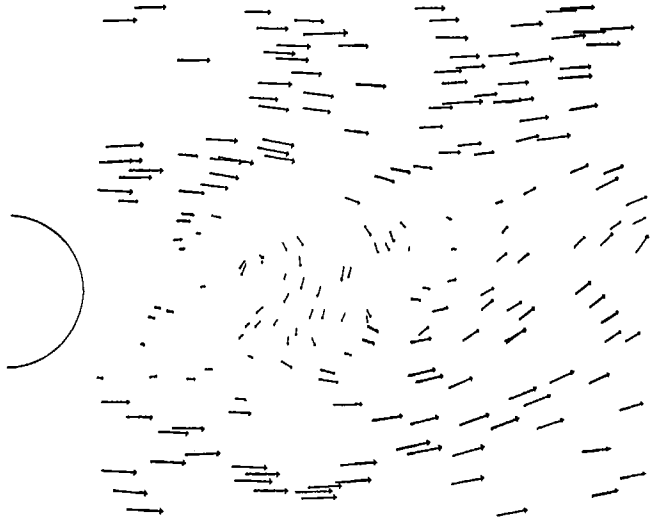

FIGURE 3. Superposition of figure 2 and the velocity field from the same phase in the next cycle.

superimposed case. It was felt that the possible error caused by superimposing two velocity fields from the same phase of successive shedding cycles was outweighed by the benefits of having more velocity vectors per frame. To assess the accuracy of the scheme, a 'bootstrap' technique similar to that described by Agüí & Jiménez (1987) was used. This technique used the interpolation scheme to find the velocity at the position of each of the interpolated vectors. The interpolated velocity was then compared to the velocity measured at that point, allowing the optimum window width and accuracy to be assessed. The optimum window width was based on the results from the interpolation in several frames.

To judge the accuracy of the vorticity measurements relative to contemporary techniques, the divergence $E$ was defined as

$$E = \partial u/\partial x + \partial v/\partial y.$$

It can be seen that the divergence is the departure from the two-dimensional continuity equation; in the perfect case $E$ should be zero. This quantity is useful since it is calculated in a similar fashion to the vorticity. In their estimate of accuracy, Nguyen Duc & Sommeria (1988) normalized the divergence with half of the difference between maximum and minimum values of vorticity. They found that 95% of grid points produced a divergence of less than 10%. When applied to the present results and using the optimum value of $H$, the respective figures were 80% and 10%. Thus, the present technique produced results of inferior accuracy to those of Nguyen Duc & Sommeria, although the present technique involved less manual processing.

Imaichi & Ohmi (1983) normalized the divergence with the free-stream velocity. Under the optimum conditions they found an average error of 2.45%. Furthermore, 88% of grid points produced an error of less than 5%. The present results yielded an average error of 2%, with 92% of grid points giving an error of less than 5%.

It is concluded that the present experimental and analysis technique gives vorticity measurements of comparable accuracy to other PSM measurements at the time the work was done. It must be conceded, however, that with more sophisticated equipment with higher resolution an improved accuracy would now be possible.

## 5. Results

For the final calculations of vorticity the measured velocity vectors were interpolated onto a $40 \times 40$ grid of points. The results presented in this section show the development of the near wake as a function of time over half a shedding cycle. Flow fields at $Re = 73$ and 226 are shown.

In addition to vorticity, viscous shear stress, defined by

$$\tau = \mu(\partial u/\partial y + \partial v/\partial x)$$

was calculated from the interpolated velocity field. Shear stress has an effect which can be described in the following ways.

(i) Shear stress is responsible for the viscous transport of momentum which is an irreversible process.

(ii) Shear stress acts to dissipate the mechanical energy. There is an increase in the internal energy of the fluid. This is simply a corollary of (i). For an incompressible fluid, rate of dissipation of mechanical energy per unit mass is given by

$$\phi = 2e_{ij}\,e_{ij}/\mu\rho \quad (\tau_{ij} = \mu e_{ij})$$

(see Batchelor 1967). This contains terms other than $\tau^2$ and thus the contours of shear stress, $\tau$, do not represent the region or magnitude of the dissipation: however, the only terms in $e_{ij}\,e_{ij}$ which contain $\partial u/\partial y$ are those in $\tau^2$ and these are the most significant as far as vortex splitting is concerned.

(iii) Shear stress causes shear strain which is the non-rigid body deformation of a fluid element. It describes how the fluid is torn apart.

The areas of the flow field affected by the shear stress and how they change with $Re$ are of interest.

The vorticity contours, non-dimensionalized with $D$ and the free stream speed $U$, are shown in figure 4 (*a–e*) at $Re = 73$, and figure 5 (*a–e*) at $Re = 226$. The development of a shed vortex can be seen on the negative-$y$ side of the wake in figure 4. Figures 4 and 5 cover one period, $T$, of the oscillations: the positive-$y$ portion occupies 0 to $0.4T$ whilst the negative-$y$ portions cover 0.5 to $0.9T$. On figure 4 (*a*), at $Re = 73$, the centre of the vortex that eventually sheds is at $x/D = 2.0$. In the next figure, it has moved to $x/D = 2.6$: note how a strand of vorticity bearing fluid trails behind it, connecting it to the high-vorticity region closer to the cylinder. In figure 4 (*c*) the vortex centre is at $x/D = 3.0$. The above described strand of vorticity has considerably decreased in extent, although a substantial region of high-vorticity fluid still exists close to the cylinder. (The structure at $x/D = 1.0$ at the bottom of this figure is the result of spurious data. One particularly inaccurate velocity vector may produce such an effect.) In figure 4 (*d*) the vortex has proceeded further downstream. The strand of vorticity still connects it to the high-vorticity-bearing fluid closer to the cylinder, although it is now very weak and the vorticity contours are not shown. In the final figure of the sequence, the vortex centre has disappeared out of the field of view.

The development of the structure downstream of $x/D = 1.0$ on the positive $y$-portion of figure 4 (*c*) is interesting. In the next figure it has retained its coherent form, although in figure 4 (*e*) it appears as two smaller structures next to one another. Further development then follows the above description for the other side of the wake and it is the downstream-most portion of the vorticity-bearing fluid that is shed into the far wake. It is at this point that the reason for presenting shear stress measurements becomes clear; the shed vortex appears to develop from the area of

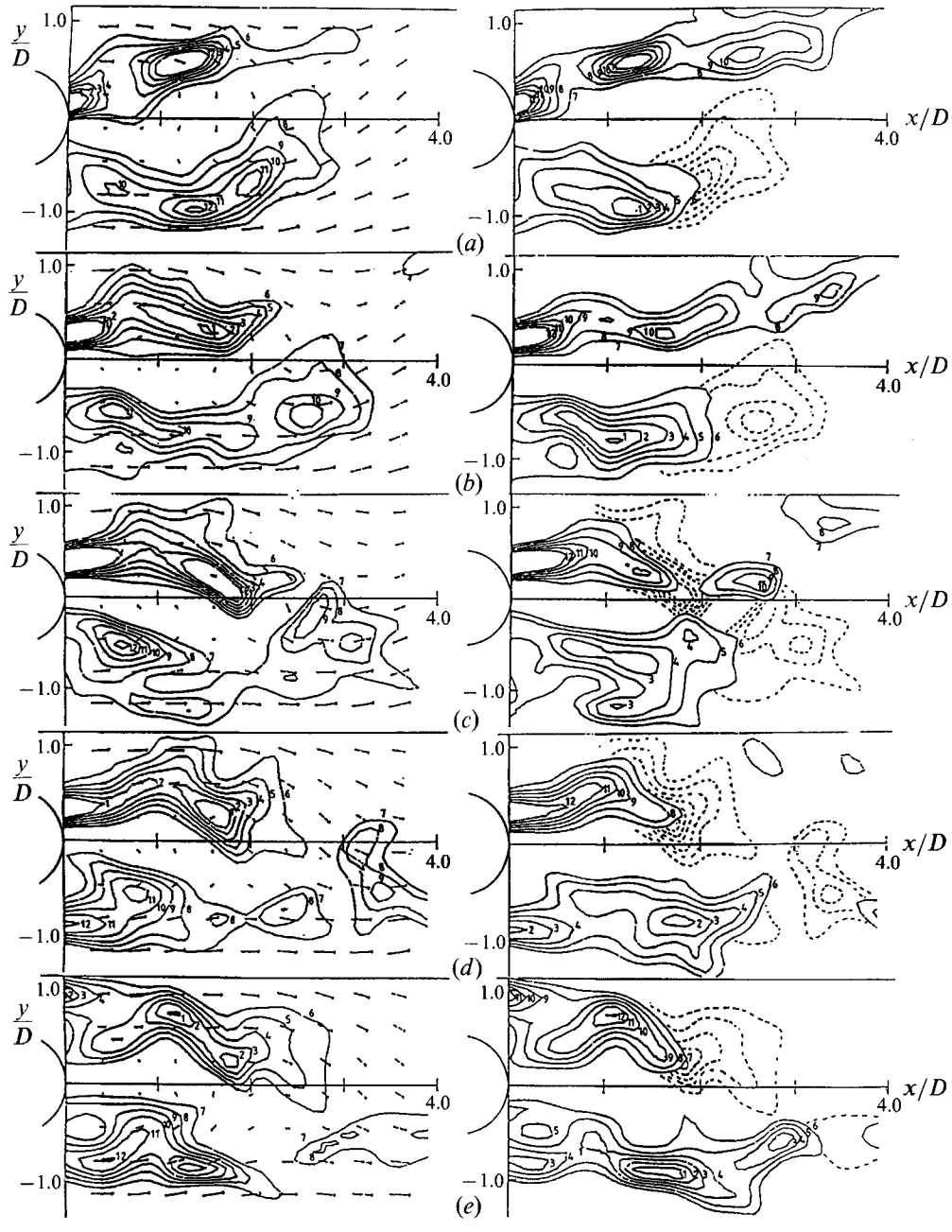


FIGURE 4. Non-dimensional vorticity and shear stress at $Re = 73$. (*a*), (*b*), (*c*), (*d*), (*e*) are separated by 0.1 shedding periods. The $x$- and $y$-axes are marked in $1D$ intervals and $x$ is measured from the rear of the cylinder. Contours of vorticity $\zeta^* = \zeta D/U$ are shown on the left and partially as dashed lines on the right where the full lines represent shear stress $\tau^* = 2\tau/\rho U^2$. Contour values are shown in table 1.

vorticity-bearing fluid that is least affected by the viscous shear stress, i.e. the region downstream of the limiting shear stress contour plotted on each of the above figures, and the splitting of the vorticity 'blob' over figures 4(*c*), 4(*d*) and 4(*e*) described above represents the effect of shear stress. Also interesting to note is the way that

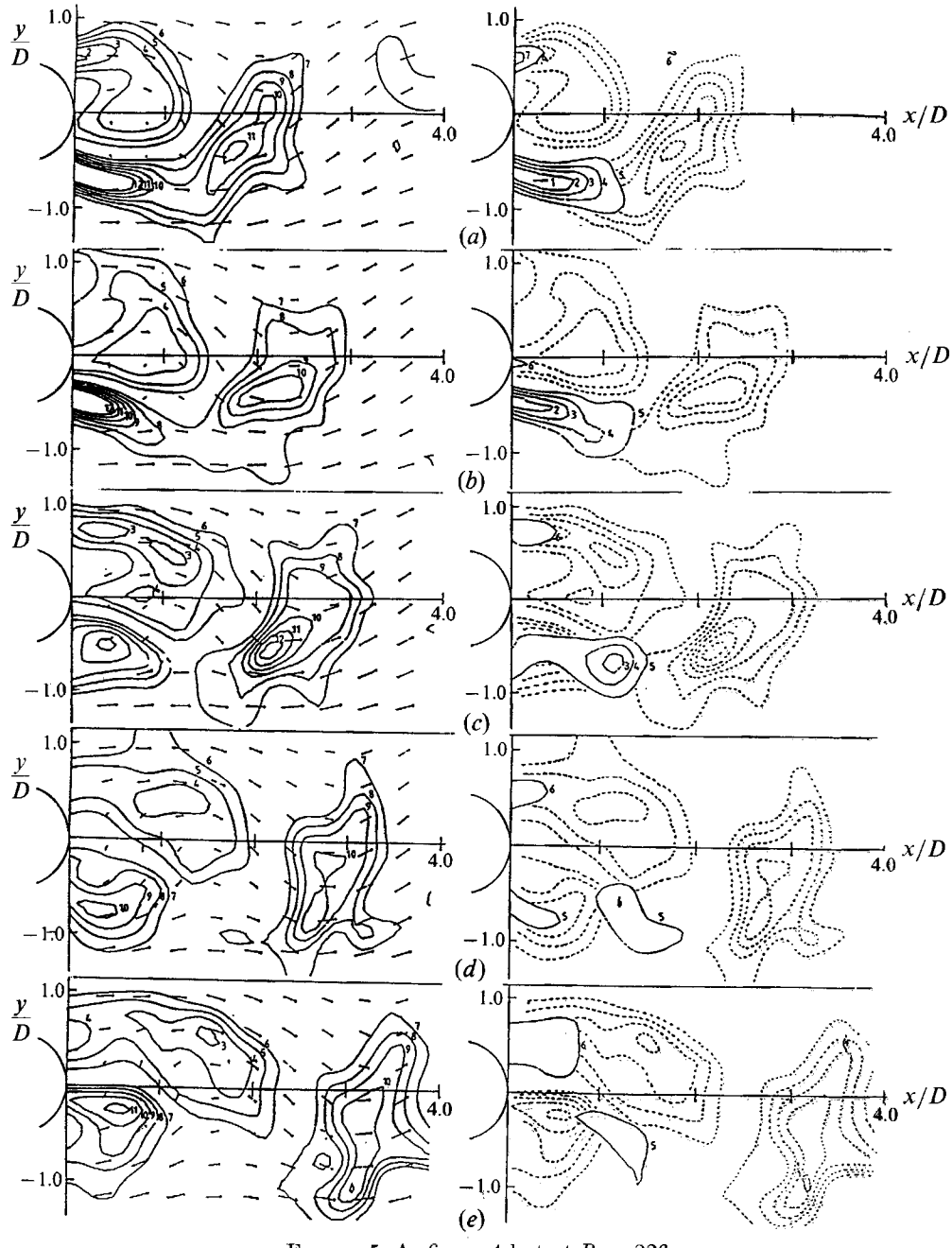


FIGURE 5. As figure 4 but at $Re = 226$.

very little positive vorticity is convected to the other side of the wake (i.e. onto the positive-$y$ portion). The shear stress in figures 4 and 5 is non-dimensionalized as indicated in the caption to the figures.

Figure 5($a$–$e$) shows the vorticity contours at $Re = 226$. In figure 5($a$) a growing vortex can be seen on the negative-$y$ side of the picture at $x/D = 1.8$. A strand of vorticity connects it to the vorticity-bearing fluid closer to the cylinder. Note the way in which the vortex has been partially pulled across to the other side of the wake.

| | $\zeta^*$ | | $\tau^*$ | |
|---|---|---|---|---|
| Contour number | *Re* 73 | *Re* 226 | *Re* 73 | *Re* 226 |
| 1 | −2.51 | −4.13 | −0.069 | −0.052 |
| 2 | −2.30 | −3.50 | −0.060 | −0.043 |
| 3 | −1.88 | −2.86 | −0.052 | −0.034 |
| 4 | −1.57 | −2.23 | −0.043 | −0.026 |
| 5 | −1.25 | −1.59 | −0.034 | −0.017 |
| 6 | −0.94 | −0.95 | −0.026 | 0.017 |
| 7 | 0.94 | 0.95 | 0.026 | 0.026 |
| 8 | 1.25 | 1.59 | 0.034 | 0.034 |
| 9 | 1.57 | 2.23 | 0.043 | 0.043 |
| 10 | 1.88 | 2.86 | 0.052 | 0.052 |
| 11 | 2.30 | 3.50 | 0.060 | |
| 12 | 2.51 | 4.13 | 0.069 | |

TABLE 1. Contour values of figures 4 and 5

In the next figure the vortex is at $x/D = 2.2$ and the connecting strand of vorticity has weakened considerably. In figure 5(*c*), the vortex is at roughly the same position, although the connecting strand of vorticity is very weak and no contours are shown. The following two figures show the vortex moving away from the cylinder and at the same time the high-vorticity region closer to the cylinder on the same side of the wake recedes. High shear stress only exists in the region of the fluid directly behind the cylinder, and the shedding vortex appears to be affected by it for only a very short time.

## 6. Discussion

The above descriptions show how a shed vortex develops from the concentrated area of vorticity in the near wake. Within the small range of Reynolds number investigated, major changes take place. To summarize, these are as follows.

(i) At $Re = 226$, the vortex is dragged further over onto the opposite side of the wake than at $Re = 73$. Figure 6 shows the variation of the maximum crossflow velocity component at $x/D = 1.0$ as a function of $Re$. At $Re = 226$, it is some 3.5 times higher than at $Re = 73$. Thus convection of the vorticity across the wake centreline is more effective at $Re = 226$ than at $Re = 73$.

(ii) At $Re = 73$ there is a substantial area of low vorticity in the near wake between the high-vorticity areas emanating from the shoulders of the cylinder (i.e. around the wake centreline). At $Re = 226$, this area is much less extensive. This change reflects the decreasing effectiveness of diffusion of vorticity as $Re$ increases; the low-vorticity area is the result of cancellation of vorticity as that of one sign diffuses into the other. At low $Re$, diffusion has time to act, so the area of low vorticity is large.

(iii) The strand of vorticity-bearing fluid trailing behind a shedding vortex is weaker and less persistent at $Re = 226$ than at $Re = 73$; at $Re = 73$, a vortex is weakening as it sheds, while the rate of attrition at $Re = 226$ is much less. This appears to tie in with the observed changes in shear stress; the strand of vorticity lies approximately within the area affected by high shear stress, and the results at $Re = 100$ and 152 (not shown in this paper, although they are described by Green 1989) reflect the above trend. Viscous shear stress results in retarded fluid motion and the vortex splitting observed by Freymuth *et al.* (1986) and Gerrard (1978) where at low

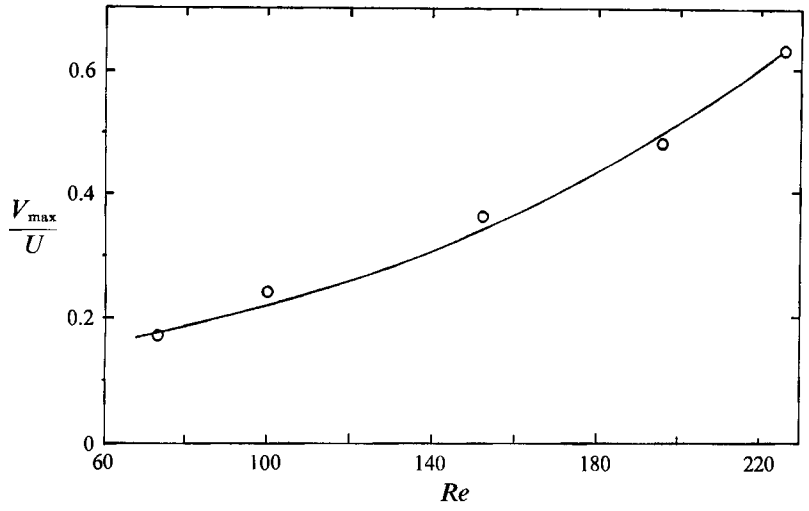


FIGURE 6. The maximum crossflow velocity component measured at $x/D = 1.0$ as a function of Reynolds number.

*Re* the vortex appeared to split apart as it shed, while at higher *Re* the observed effect was much reduced. Thus the role of the fluid left behind in the near wake as the vortex splits is important since it contains vorticity that would otherwise have been shed.

### 6.1. *A low-Reynolds-number vortex shedding mechanism*

Williamson (1989) proposed a universal Strouhal number/Reynolds number relationship which applies through the *Re* range discussed here. Although the Strouhal number *S* increases with increasing *Re*, the rate of increase decreases, with *S* tending towards a constant value at high *Re*. Thus, the fundamental nature of the wake changes as *Re* increases, and it is proposed that the changes in vorticity transport account for the change in shedding frequency. Ultimately these are linked with the decrease in the effectiveness of viscosity and of diffusion as *Re* increases. The differences described at the beginning of this discussion quantify these effects.

The flow field may be described as being in a continuous state of transition, from one at very low *Re*, where the shear stress dominates the near wake and vortex splitting characterizes the near-wake behaviour, to a high-*Re* state where the near-wake behaves as described by Gerrard (1966). The solution of the two-dimensional Navier–Stokes equations over the same range of Reynolds number shows vorticity distributions similar to those observed. This suggests that the principal characteristics of the near wake are determined by two-dimensional processes.

We consider now the physical mechanisms which occur in the near wake. Vorticity from the separated boundary layers accumulates in the wake. Circulation is lost by diffusive mixing of vorticity of opposite signs, otherwise the equal and opposite circulation on the two sides of the wake remains constant. The convection of vorticity by the spatially varying velocity field redistributes the vorticity. Close to the cylinder the regions of high shear in the near wake are the remnants of the boundary-layer shear. Further downstream at low Reynolds number the regions of high shear indicate where the vorticity-bearing fluid is undergoing the vortex splitting process. After a time, which depends upon the rate of supply of vorticity and the extent of the shear stress, a buildup of vorticity outside the high-shear-stress area develops. Owing to the comparative lack of energy dissipation, this 'blob' of

vorticity maintains a coherent structure. A 'vortex' is thus formed, which has its own entrainment effects. The vortex can feed itself as well as induce crossflow from the other side of the wake. In this way the vortex ultimately cuts itself off from the influence of the near wake and is effectively shed. The vortex shedding process therefore, takes place in two consecutive parts, i.e. vortex formation followed by actual vortex shedding. At very low $Re$ vortex formation is the crucial process, and ultimately the vortex shedding frequency is determined by how long it takes for a sufficiently organized vortical structure to develop outside the influence of high shear stress. As $Re$ increases, the area occupied by viscous shear stress decreases, so the development time associated with this aspect becomes shorter, leading to a higher shedding frequency. At high enough $Re$, the significance of the shear stress contribution becomes so small that the shedding frequency is governed by the vortex-induced velocity field, and the Strouhal number tends to a constant.

### 6.2. *The formation region length at low Reynolds number*

From the above we can describe the mechanism of vortex formation at low Reynolds number and its variation with Reynolds number. The formation region length has generally been defined as being the distance from the rear of the cylinder to the position of the centre of the vortex when it is shed. At high Reynolds number the position of shedding is where the vortex has maximum strength. At low Reynolds number, shedding is a more protracted process. An important moment in the vortex shedding cycle is when the concentration of vorticity in the near wake first splits into the portion that remains in the wake and the portion which is, in part, eventually shed. This first appearance of vorticity concentration is seen in the negative-$y$ parts of figures 4($c$) and 4($d$) at $Re = 73$: the vortex is at $0.7D$ and a saddle point at $0.5D$ in figure 4($d$). At positive-$y$ in figures 5($a$) and 5($b$) the saddle point is at $0.3D$ and the vortex at $0.75D$. Points indicating these positions are shown in figure 7. Also shown are the results of Gerrard (1978) for a definition of formation region length based on the behaviour of a filament of dyed fluid in the near wake. The present work shows that this indicates only the beginning of shedding and thus that Gerrard's definition of formation region length, $L_f$, was too small. Here we define $L_f$ as the distance to the centre of the vortex after it escapes from the region of high shear stress. At this time of shedding, vortex splitting has taken place at the lower Reynolds number of 73 and much of the circulation on that side of the near wake remains there or has been dissipated. The shedding is seen to occur in figure 4($b$) at negative-$y$.

At high Reynolds number there are several equivalent definitions of formation length. At a conference in 1972 Griffin (1974) suggested that formation length could be defined as ending where the longitudinal velocity fluctuation at the shedding frequency had its maximum amplitude. This quantity has been measured at low Reynolds number by Kovasznay (1949), Schaefer & Eskinazi (1959), Griffin (1974), Griffin & Ramberg (1975) and Nishioka & Sato (1978). Their results are shown in figure 7 (Kovasznay's value is at $x/D = 6.5$ at $Re = 56$), and show a spread of values. We have analysed our results to determine the position of maximum vortex strength. This was determined from the position at which vorticity times vortex area was a maximum. The position of maximum strength and of the escape of the vortex from the shearing region were found to be the same and in agreement with the values obtained by the other workers (as well as their results agree with each other).

We see, therefore, that the position of maximum strength of the vortex, not surprisingly, marks the end of the formation region at both high and low Reynolds

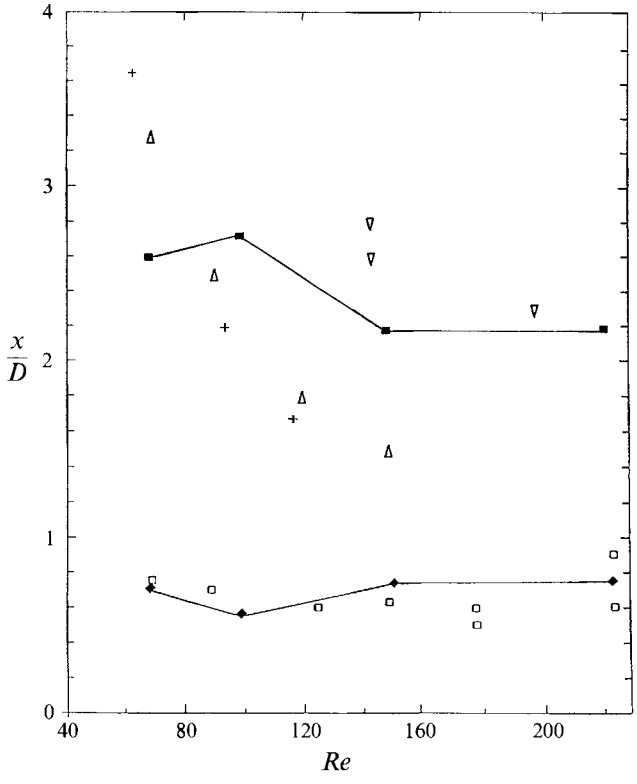


FIGURE 7. Developments in the near wake as a function of the distance, $x$, downstream of the rear of the cylinder. Present results: ◆, formation of separated area of vorticity which is eventually partially shed; ■, position of vortex centre when beyond the shear stress region and also position of maximum vortex strength. Results of other workers: □, formation region length (Gerrard 1978). Position of maximum longitudinal velocity amplitude: +, Schaefer & Eskinazi (1959); △, Nishioko & Sato (1978); ▽, Griffin (1974), Griffin & Ramburg (1975).

numbers. We have demonstrated in the present work the different mechanics of the vortex shedding process at low Reynolds number. Shearing stress and vortex splitting characterize the lower Reynolds numbers of the range we have investigated. Shear is not particularly in evidence at $Re = 226$ where the mechanism of shedding is essentially the same as it is at much higher Reynolds number. The principal difference being that at this low Reynolds number the vortex does not grow in a fixed position before it is shed.

### 6.3. *Vortex strength in the near wake*

From the vorticity fields as depicted in figures 4 and 5 it is possible by integration to determine the shed vortex strength. In figure 8 the results of this integration are compared with the vortex strength determined by Green & Gerrard (1991) and the agreement is good. This vortex strength was determined from the finding that the vortex pressure distribution was that of an Oseen vortex (as found by Schaefer & Eskinazi 1959) and matching this distribution to the surface contour to determine the strength and age of the vortex. The error bars are an estimate of the accuracy of the integration. The results were obtained in different towing tanks but with the same drive arrangement. Also shown on this figure are the results of two solutions of the two-dimensional Navier–Stokes equations (Burrows 1990 and Pao, Stevenson &

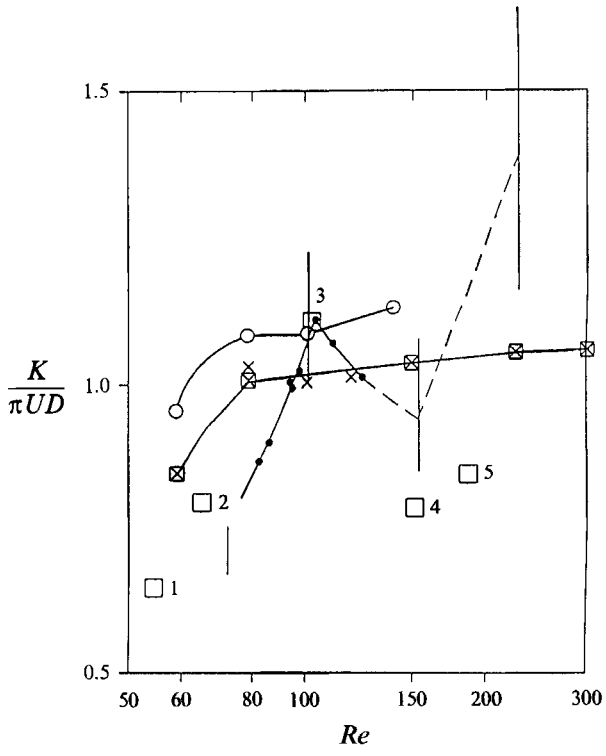


FIGURE 8. Vortex strength, $K$, as function of Reynolds number: ●, Green & Gerrard (1991); |, integration of present vorticity contours; ×, two-dimensional numerical solution, Burrows (1990); ⊠, present computations; ○, two-dimensional numerical solution, Pao *et al.* (1990); □: 1, 3, Thom (1933); 2, Schaefer & Eskinazi (1959); 4, Berger (1964); 5, Timme (1957).

Nicolaou 1990). At $Re = 100$ the agreement between the numerical analysis and our experiments is good but in the range shown there is no indication in the computed strengths of the relatively large undulation observed experimentally. In this range of Reynolds number it is well known that three-dimensional effects have been observed. At $Re < 100$ in our experiment the vortices are known to be shed straight and parallel to the cylinder axis (Slaouti & Gerrard 1981). At $Re > 120$ streamwise vorticity due to some three-dimensional instability has been observed. Calculation shows that the consequent changes in the velocity field at the water surface, which is locally two-dimensional anyway, is only a small effect. It must be conceded that the presence of three-dimensionalities could produce a different shedding mechanism even at the surface.

Also plotted in figure 8 are the experimental results of four other workers which show good agreement with the present experimental values. Figure 9 shows the lift coefficient amplitudes, $C_L$, measured by Tanida, Okajima & Watanabe (1973) which follow the sharp fall as Reynolds number decreases below 100. Flow visualization (e.g. Gerrard 1978) shows that the wake vortices increase from zero strength at the critical Reynolds number in agreement with the trend of the experimental results in figure 8. The experimental results are clearly in agreement with each other at $Re <$ 150 but could, of course, all be subject to some three-dimensional effect of, as yet, unknown mechanism. The vortex strengths determined by numerical analysis could fall to zero at a similar Reynolds number. The amplitudes of the computed lift

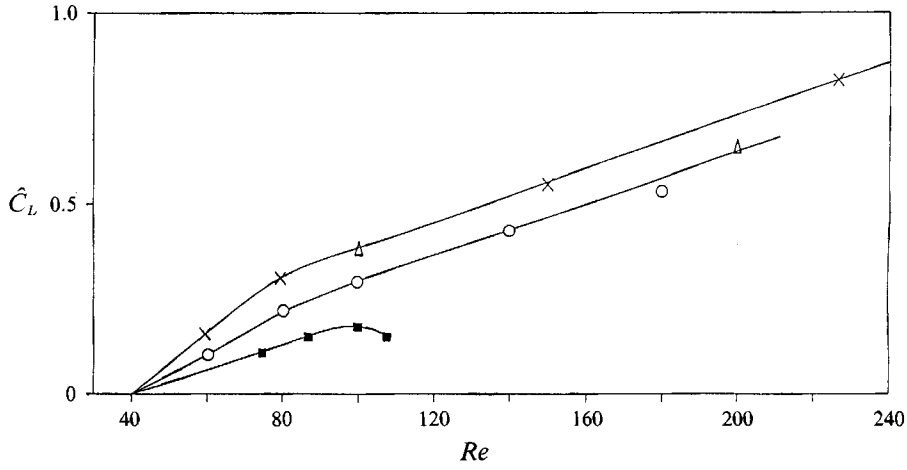


FIGURE 9. Amplitude of lift coefficient as a function of Reynolds number: ○, Pao *et al.* (1990); △, Benson *et al.* (1989); ×, Burrows (1990) and present computations; ■, Tanida *et al.* (1973).

coefficient shown in figure 9 clearly extrapolate to zero at a Reynolds number of about 40. The vortex strength values of Pao *et al.* (1990) were determined from graphical integration of vorticity contours and are therefore subject to the same uncertainty as the present results. Transverse oscillations of a cylinder force two-dimensional shedding across the whole span. The cross-stream velocity fluctuation behind the cylinder induces a high-Reynolds-number type of shedding, reduces the formation length and increases the vortex strength. This is thought to be the result of the cylinder oscillation rather than the two-dimensionality.

The numerical results of Pao *et al.* (1990) were determined from an implicit finite-difference solution of the flow started from rest. The computation was subject to the small disturbances of numerical noise and truncation errors. At the higher Reynolds numbers the wake oscillation soon grows to a steady amplitude and constant shed vortex strength. At $Re = 60$, on the other hand, the flow progresses to a form similar to that shown in figure 4 and reaches a steady oscillating state after 200 diameters of travel of the cylinder. In the work of Green & Gerrard (1990) measurements were made after 500 diameters of travel and in the present work after 100 diameters of cylinder motion from rest. The computational scheme of Burrows (1990) is a vortex method with splitting of the convection and diffusion terms in the equations of motion. The oscillations were started by including a vortex in the wake. The magnitude of the oscillating quantities soon became independent of the strength of this vortex. The vortex strengths were determined by numerical integration of the wake vorticity, in this case after only some 20 diameters of travel of the cylinder. We have repeated these computations for larger distances of travel at the Reynolds numbers indicated in figure 8 and obtained the vortex strengths from a line integral across the wake at 10 diameters downstream of the cylinder centre. This circumvents the difficulty and small error in deciding on the spatial limits of the vortices. The numerical results (figure 8) show a constant value of $K/\pi UD$ at $Re > 80$. It follows that the increase of the $C_L$ values with increasing Reynolds number is due to the changing vortex development in the near wake. Computed $C_L$ values continue to rise to $Re > 1000$.

The major discrepancy between experimental results and those of two-dimensional computation is only at the highest Reynolds number in the present range. In view

of the limit of accuracy of the present method the clarification of the cause of the discrepancy must await further work in the Reynolds number range. At higher Reynolds numbers two-dimensional computation fails to reproduce the appearance of a lengthened formation region which is found in experiments.

## 7. Conclusions

A particle tracer technique was developed for application to bluff-body wakes at low Reynolds numbers. The manual processing burden common to such techniques was reduced to a minimum and vorticity was measured to a reasonable accuracy. Shear stress was calculated from the measured velocity field.

Changes in the vortex shedding cycle were observed as $Re$ increased. At very low $Re$ the shedding cycle was characterized by vortex splitting and high shear stress over a wide area of the near wake. At higher $Re$ vortex splitting was less apparent, reflected by the lower shear stress. The shear stress measurements quantify previous descriptions of vortex splitting. The low-Reynolds-number vortex shedding mechanism was described, in which the vortex shedding frequency is determined by the length of time associated with initial vortex development, which is influenced by the extent of the shear stress, and the time required for the vortex to further develop and escape into the far wake. The formation region length was found to follow a definition applicable at all Reynolds numbers. Its end is characterized by the position of the vortex centre at which the vortex strength is a maximum. This was also found to be where the vortex finally escapes from the region of shear stress in the near wake. The vortex strength was calculated from the vortex contours and found to be in agreement with other experimental results. Comparison with the results of two-dimensional numerical analysis shows fair agreement at $Re \leqslant 150$. At the highest Reynolds number of 226 there is a difference between experiment and computation. In view of the not very accurate values of the vorticity it is possible that the difference is due to experimental error but may also be contributed to by the omission of turbulence from the numerical analysis. The resolution of the discrepancy must await more accurate measurements of vortex strength in this Reynolds number range.

The authors would like to take this opportunity to thank the staff at the Goldstein Aeronautical Engineering Laboratories, University of Manchester for their technical assistance. The first author acknowledges the financial support of the Science and Engineering Research Council. We also gratefully acknowledge the receipt of equipment funds from the Science and Engineering Research Council and the Medical Research Council.

## REFERENCES

Agüí, J. C. & Jiménez, J. 1987 On the performance of particle tracking. *J. Fluid Mech.* **185**, 447.

Al-Khafaji, A. A. 1989 Instabilities in the near wake of a circular cylinder at low Reynolds numbers. Ph.D. thesis, University of Manchester, UK.

Anagnostopoulos, E. & Gerrard, J. H. 1976 A towing tank with minimal background motion. *J. Phys.* E: *Sci.* Instrum. **9**, 951.

Batchelor, G. 1967 *An Introduction to Fluid Dynamics.* Cambridge University Press.

Benson, M. G., Bellamy-Knights, P. G., Gerrard, J. H. & Gladwell, I. 1989 A viscous splitting algorithm applied to low Reynolds number flow around a circular cylinder. *J. Fluids Struct.* **3**, 439.

Berger, E. 1964 The determination of the hydrodynamic parameters of a Karman vortex street from hot-wire measurements at low Reynolds numbers. *Z. Flugwiss.* **12**, 41.

BLOOR, M. S. 1964 The transition to turbulence in the wake of a circular cylinder. *J. Fluid Mech.* **19**, 290.

BURROWS, A. P. 1990 The flow past bluff bodies by a vortex method. Ph.D. thesis, Manchester University, UK.

FREYMUTH, P., FINAISH, F. & BANK, W. 1986 Visualisation of the vortex street behind a circular cylinder at low Reynolds number. *Phys. Fluids* **29**, 1321.

GERRARD, J. H. 1966 The mechanics of the formation region of vortices behind bluff bodies. *J. Fluid Mech.* **25**, 401.

GERRARD, J. H. 1967 Numerical computation of the magnitude and frequency of the lift on a circular cylinder. *Phil. Trans. R. Soc. Lond.* A **261**, 137.

GERRARD, J. H. 1978 The wakes of cylindrical bluff bodies at low Reynolds numbers. *Phil. Trans. R. Soc. Lond.* A **288**, 351.

GREEN, R. B. 1989 Measurements of vorticity and vortex strength in the wake of a circular cylinder at low Reynolds numbers. Ph.D. thesis, University of Manchester, UK.

GREEN, R. B. & GERRARD, J. H. 1991 An optical interferometric study of the wake of a bluff body. *J. Fluid Mech.* **226**, 219.

GRIFFIN, O. M. 1974 Effects of synchronised cylinder vibration on vortex formation and mean flow. In *Flow Induced Structural Vibrations. IUTAM-IAHB Symp. Karlsruhe Aug. 1972* (ed. E. Naudascher). Springer.

GRIFFIN, O. M. & RAMBERG, S. E. 1975 Vortex shedding from a cylinder vibrating in line with an incident flow. *J. Fluid Mech.* **75**, 257.

IMAICHI, K. & OHMI, K. 1983 Numerical processing of flow visualisation pictures – measurement of two-dimensional vortex flow. *J. Fluid Mech.* **129**, 283.

KOVASZNAY, L. S. G. 1949 Hot-wire investigation of the wake behind cylinders at low Reynolds number. *Proc. R. Soc. Lond.* A **198**, 174.

NISHIOKA, M. & SATO, H. 1978 Mechanism of determination of the shedding frequency of vortices behind a cylinder at low Reynolds numbers. *J. Fluid Mech.* **89**, 49.

NGUYEN DUC, J. M. & SOMMERIA, J. 1988 Experimental characterisation of steady two-dimensional vortex couples. *J. Fluid Mech.* **192**, 175.

PAO, L. Y., STEVENSON, T. N. & NICHOLAOU, D. 1990 On the vorticity shed by a circular cylinder at Reynolds numbers around 100. *Department of Engineering, University of Manchester, Internal Rep. Aero.* 9010.

SCHAEFER, J. & ESKINAZI, S. 1959 An analysis of the vortex street generated in viscous fluid. *J. Fluid Mech.* **6**, 241.

SLAOUTI, A. & GERRARD, J. H. 1981 An experimental investigation of the end effects on the wake of a circular cylinder towed through water at low Reynolds numbers. *J. Fluid Mech.* **112**, 297.

TANIDA, Y., OKAJIMA, A. & WATANABE, Y. 1973 Stability of a circular cylinder oscillating in uniform flow or in a wake. *J. Fluid Mech.* **61**, 769.

THOM, A. 1933 The flow past circular cylinders at low speeds. *Proc. R. Soc. Lond.* A **141**, 651.

TIMME, A. 1957 On the velocity distribution in vortices. *Ing. Arch.* **25**, 205.

WILLIAMSON, C. H. K. 1989 Oblique and parallel modes of vortex shedding in the wake of a circular cylinder at low Reynolds numbers. *J. Fluid Mech.* **209**, 579.